Effects of nonlinear Shear on the Dynamics of a Counter- Rotating Vortex Pair

Thomas Hofbauer & Thomas Gerz

Institute of Atmospheric Physics, DLR Oberpfaffenhofen
D-82234 Weßling, Germany

ABSTRACT

Numerical simulations were conducted to investigate the influence of nonlinear vertical shear on the trajectories of a trailing vortex pair. Descending vortices which approach a shear layer begin to tilt and diverge. It is shown that the vortex whose vorticity is of opposite sign to the shear–layer vorticity can stall or even rebound, whereas the other vortex penetrates through the shear layer. The behaviour of the vortices is highly sensitive to the vorticity distribution within the shear layer and cannot be described by circulation or maximum vorticity relations.

When the vorticity distribution of the shear layer varies along the axis of the vortices, the interaction between shear and vortex is also modified in axial direction and presumably triggers a quickly growing instability of the vortex pair.

INTRODUCTION

As a consequence of lift, aircraft generate counter-rotating pairs of trailing vortices which are considered of being hazardous to following aircraft. With the introduction of large aircraft such as the Boeing 747 thirty years ago, the number of air traffic incidents and accidents due to wake vortex encounters severely increased. In order to improve flight safety, many investigations on aircraft wake vortices were performed which eventually led to internationally applied separation standards (Hallock *et al.*, 1998). These regulations prescribe the minimum separation distance between leader and follower aircraft during take-off, approach, and landing. They are exclusively based on the maximum take-off weight of the aircraft. Subsequent studies, however, emphazised that decay and trajectory of wake vortices and, hence, their hazardousness strongly depend on the atmospheric conditions. It is evident that the separation standards are rather conservative guesses in many meteorological situations. On the other hand, these standards limit the throughput capacity of some major airports already today. Driven by the increase of the world's air traffic, this situation will become more severe in the next future. Therefore, attempts are underway which aim at optimizing the separation standards by taking into account the meteorological conditions.

The main atmospheric parameters that influence vortex lifetime and trajectories are turbulence, thermal stratification, crosswind and wind shear. In a quiescent environment, the vortices descent due to their mutual velocity induction. This is an advantagious property because they descend below the glide path which all aircraft have to follow when approaching an airport. However, owing to, e.g., LIDAR measurements at Heathrow airport (Greenwood and Vaughan, 1988), there is evidence that thermal stratification and crosswind shear can prevent the descent or even cause an ascent of the

vortices back to the flight level. Based on the measurements at Memphis and at Idaho Falls, Proctor (1996) and Proctor *et al.* (1997) studied this behaviour by means of numerical simulations. Here, we continue their attempt and focus on the role of shear layers (vertical variations of horizontal wind, $U(z)$) with different vorticity distributions. We consider shear layers where U increases monotonically from one constant value to another value within a given height interval and shear layers in form of low-level jets as often observed in early morning boundary layers. Results of two-dimensional and three-dimensional Navier-Stokes simulations will be presented.

NUMERICAL SOLUTION TECHNIQUE

Numerical Method and Boundary Conditions

The numerical model used in this study solves the full set of Navier-Stokes equations in its conservative form for an incompressible fluid. Time advancement is performed by a prognostic step for advection and diffusion using the second-order Adams-Bashforth scheme followed by a diagnostic step which solves the Poisson equation for the dynamic pressure. On a staggered grid, the spatial derivatives are approximated by explicit second-order central finite differences. The model exhibits the property of being nondissipative and weakly dispersive. A description of the model can be found in Schumann *et al.* (1987).

The coordinates of the computational domain are defined by the vortex system: x, y, and z are the spanwise, axial, and vertical directions, respectively. Rigid-lid and free-slip boundary conditions are used for the bottom and the top of the computational domain. For the boundaries in spanwise direction, inflow and outflow conditions are implied and periodicity is assumed in axial direction.

Vortex Initialization

The wake vortex pair generated by aircraft is the result of the rollup process of the vortex sheet which is shed by the lifting wing. As we are interested in the far-field characteristics we do not account for these near-field processes and start our simulation with already mature vortices. The simulations are initialized by the linear superposition of two counterrotating Lamb-Oseen vortices with circulation $\Gamma_0 = \pm 250\, m^2/s$ and separation $b_0 = 24\, m$.

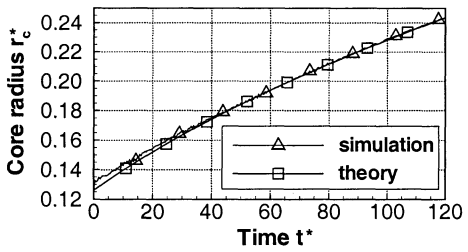

Figure 1: Core radius growth

The vortices are embedded in different background shear flows, as described below. In the following, quantities marked with an asterisk are normalized using Γ_0 and b_0 as reference scales. The tangential velocity V_θ^* of a solitary Lamb-Oseen vortex is given as a function of radius r^* with respect to its center by

$$V_\theta^*(r^*) = \frac{1}{2\,\pi\, r^*}\left(1 - e^{-\beta(r^*/r_c^*)^2}\right) \qquad (1)$$

where $r_c^* = 1/8$ is the initial core radius and $\beta = 1.2564$ is a constant. Common to all simulations are the Reynolds number $\Gamma_0/\nu = 4400$ (ν is the kinematic viscosity) as well as the grid spacing in spanwise and vertical direction $\Delta x^* = \Delta z^* = 1/24$. The initial vortex core diameter is therefore resolved by 6 grid cells.

Accuracy

The described model has proven its reliability in various studies related to microscale and mesoscale meteorological problems (see, e.g., Dörnbrack and Dürbeck, 1998). In order to validate the model for wake vortex issues, we analyze the diffusion of a vortex, i.e. the growth of its core radius, and compare the results with the analytical solution $r_c = 2(\beta\nu(t + t_0))^{1/2}$. Here, t_0 is the time, a potential vortex would need to diffuse to a vortex whose core size is equal to the initial core size of our simulation. The good agreement is evident from Figure 1. Due to computer constraints we are restricted to very low Reynolds numbers compared to "real life" circulations and viscosities. Nevertheless, a Reynolds number variation by Darracq *et al.* (1999) showed that the interaction between shear layer and vortex as well as the vortex trajectories are almost independent of the Reynolds number.

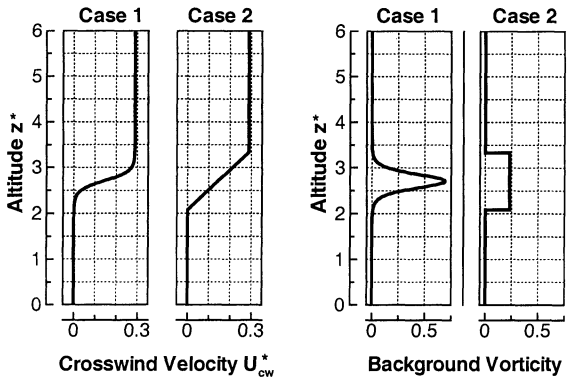

Figure 2: Crosswind profile and vorticity profile of shear layer for cases 1 and 2

POSITIVE SHEAR

In this section, we consider two different cases of shear layers. For the first case we assume a crosswind profile which follows a hyperbolic tangent function of altitude z^* of the form

$$U^*_{cw}(z^*) = U^*_{max}\frac{1+\tan^{-1}\left(c\,(z^*-z^*_0)\right)}{2}\,, \qquad (2)$$

see Figure 2. The crosswind shear results in a shear layer with mid-altitude $z^*_0 = 2.7$. Far below and far aloft z^*_0, there is no crosswind and crosswind of magnitude $U_{max} = 3\,m/s = 0.29\,\Gamma_0/b_0$, respectively. The thickness of the transition zone can be adapted by the free parameter c which is chosen to be 0.2 here. In the second case, we slightly modify $U^*_{cw}(z^*)$ by assuming a linear behaviour of U^*_{cw} between $z^*_l = 2.1$ and $z^*_u = 3.3$. In both cases we simulate the flow in span/height cross-sections (2d). We initialize the crosswind profiles in the entire domain and keep it constant at the inflow boundary $x^* = 0$ for all time. The vortex pair is initially 2.3 b_0 above the mid altitude of both shear layers. Also shown in Figure 2 are the profiles of vorticity ω^*_y of the respective shear layers. Whereas ω^*_y is a smooth function of height with a peak value of 0.69 in case 1, it has a constant value of 0.23 throughout the shear layer in case 2. Please note that the total amount of shear layer circulation $\Gamma^*_{sl} = \int \omega^*_y\, dA^*$ is the same for case 1 and case 2.

Figure 3 now depicts the flow evolution for case 1, starting with the initial set-up. Dotted contour lines denote negative values of vorticity, i.e. the negative vortex rotates counter-clockwise. In the early stage

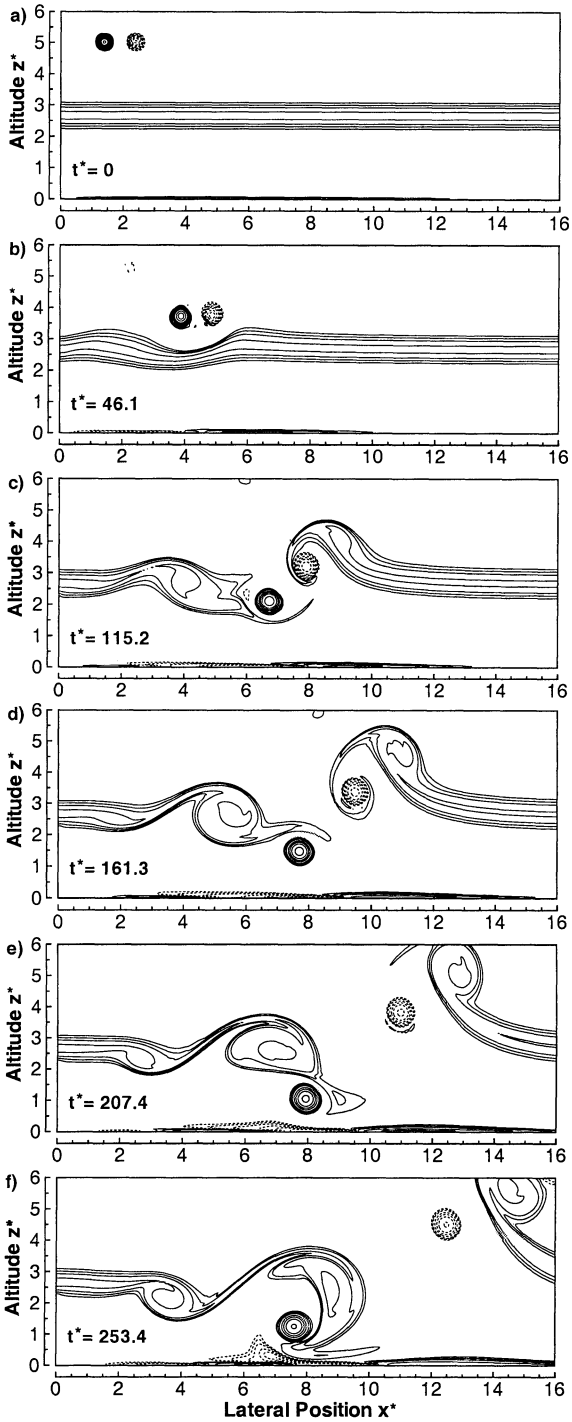

Figure 3: Evolution of case 1 in terms of vorticity contours ω^*_y in span/height cross-sections. Contour levels are plotted at $\pm 0.05, \pm 0.1, \pm 0.2, \pm 0.5, \pm 1$, and so forth. The maximal value of vorticity drops from $\omega^*_{y,max} = 22$. ($t^* = 0$) to 5.6 ($t^* = 253.4$), whereas Γ remains constant.

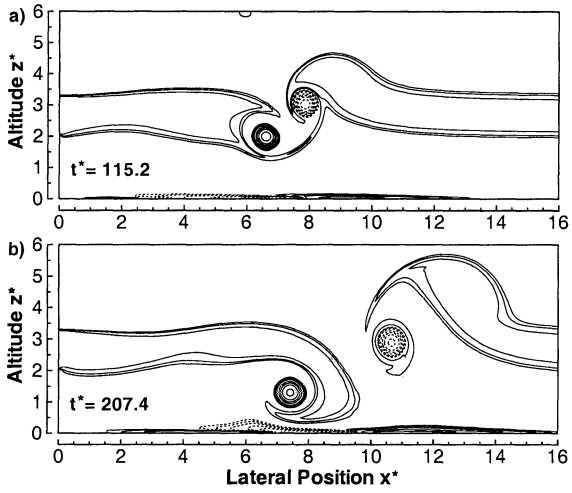

Figure 4: As Figure 1 for case 2.

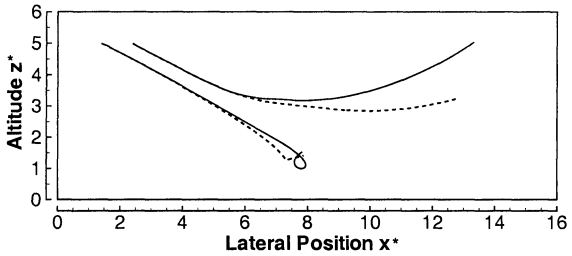

Figure 5: Vortex trajectories for case 1 (solid line) and case 2 (dashed line).

of the simulation, the primary vortices descend due to their mutual velocity induction while at the same time being advected by the prevailing crosswind. At $t^* = 46.1$ (Figure 3b) deformation of the shear layer due to the influence of the vortex pair becomes obvious. Due to ground friction tertiary vorticity is generated at the lower boundary. At $t^* = 115.2$ (Figure 3c) the vortex pair dips into the shear layer which results in the tilting of the vortex pair accompanied by a divergence of the vortices. As the vortices continue to separate (Figure 3d), the mutually induced velocity becomes weaker which in turn result in an increasing relative influence of the shear layer on each of the vortices. The shear layer which has been broken up by the vortex pair starts to roll up at its ends and forms large secondary eddies. Each of these eddies form a new vortex pair with one of the primary vortices. The downwind pair consists of counterrotating vortices which mutually induce an *upward* motion, whereas for the upwind pair both vortices rotate clockwise and, therefore,

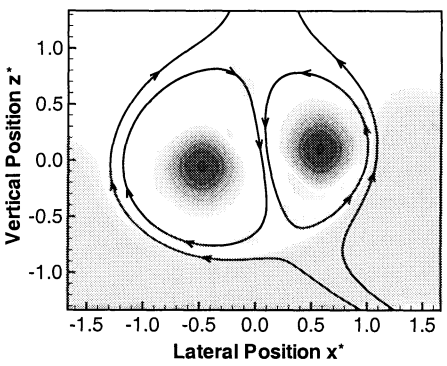

Figure 6: Flow field around the vortex pair in a moving reference frame for case 2 at $t^* = 59.1$. Levels of $|\omega_y^*|$ are illustrated by the grey scale.

tumble around each other (Figure 3e). When coming closer to the ground, the upwind pair separates tertiary vorticity of opposite sign from the ground (Figure 3f) and hence, also starts to bounce back. In Figure 4 the evolution of case 2 is shown. Comparing both cases one observes in principle similar features as tilting and divergence of the primary vortices as well as the breaking up of the shear layer. However, a closer inspection reveals that the downwind vortex does not rise again but stalls in the height of the shear layer (Figure 5). We therefore conclude that the shear layer strength in terms of shear layer *circulation* per unit length is no comprehensive measure for the rebounce phenomenon. One might therefore suspect that the observed tendency is rather related to the maximum shear layer *vorticity* which is three times higher in case 1. However, results of another simulation, where the shear layer vorticiy was even more concentrated at mid altitude than in case 1 (and thus, with a much larger peak value), showed that the vortices penetrated through the shear layer. Probably, the shear layer thickness constitutes another important parameter. An interesting view for the observed phenomena is given in a reference system that moves with the vortex oval. The vortex oval is defined by the streamlines going through the stagnation points. Hence, it represents the borderline between the outer and the inner flow field. In an early stage of the simulation of case 2, the streamline pattern around the vortex oval is symmetric, despite the prevailing crosswind. Once the vortices begin to interact with the shear layer, this symmetry breaks (Figure 6). The

shear causes a modification of the angle of attack and the vortex pair tilts. Robins and Delisi (1990) suspected that this phenomenon is due to the increased weakening of one of the vortices. Although this view appears reasonable since the ratio of upwind and downwind area of the vortex oval changes, we do not find essential differences in vortex circulation.

We argue that the observed phenomena of vortex tilting and vortex ascent can be explained by considering that the vorticity of each discrete infinitesimal area of the shear layer induces an infinitesimal velocity on the primary vortices according to the Biot-Savart law. Since the effect of velocity induction decreases with distance, the shear layer deformation causes different induced velocities for the upwind and downwind vortex which explains their differing trajectories.

LOW–LEVEL JET

In this section preliminary results of two- and three-dimensional simulations of a vortex pair subjected to a low-level jet are presented. In the three-dimensional simulation, $U^*_{cw}(y^*, z^*)$ is given by

$$U^*_{cw}(y^*, z^*) = U^*_{max}\Big(1 + cos\Big(\frac{\pi\,(z^* - z^*_0)}{\delta^*(y^*)}\Big)\Big) \quad (3)$$

with a sinusoidally varying thickness δ^* in axial direction y^* that follows

$$\delta^*(y^*) = \delta^*_{mean} - \delta^*_{var} \cdot cos\big(\,2\,\pi\,y^*/\,y^*_{max}\big) \quad (4)$$

with mean value $\delta^*_{mean} = 1.5$ and variation $\delta^*_{var} = 0.5$. The wavelength of the variation is equal to the domain size in axial direction $y^*_{max} = 4$. The maximal jet velocity amounts to $U^*_{max} = 0.4$ and is situated at $z^*_0 = 1.5$. For illustration, $U^*_{cw}(y^*_1, z^*)$ and $U^*_{cw}(y^*_2, z^*)$ are shown in Figure 7 where $y^*_1 = 0$ and $y^*_2 = y^*_{max}/2$ mark the axial positions of the maximum variation. The vortex pair has been initialized at $z^* = 3$ and the computational domain is resolved by $256 \times 64 \times 96$ grid cells.

Figure 8 shows iso-surfaces of absolute vorticity $|\vec{\omega}^*| = 0.5$ at $t^* = 80.6$. Four sheets which represent the shear layer can be seen. At the bottom of the domain, sheets of tertiary vorticity have been generated due to ground friction. In order to visualize the location and orientation of the primary

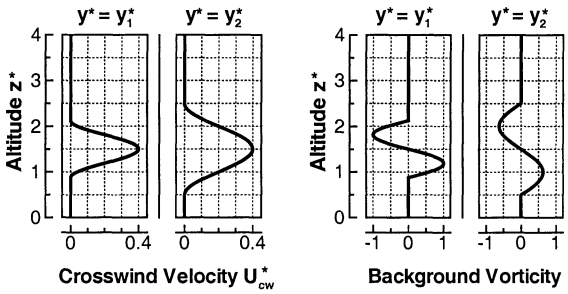

Figure 7: Crosswind profiles and background vorticity for the extrema of the variation.

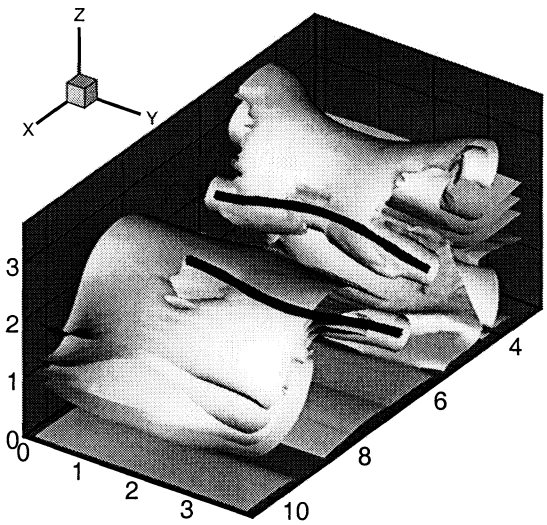

Figure 8: Isosurfaces of vorticity $|\vec{\omega}^*|$ at $t^* = 80.6$.

vortices, which are partly covered by the shear layer, a second iso-surface image with higher treshold $|\vec{\omega}^*| = 8$ has been superimposed to the first one, presenting the vortex cores as dark tubes. As expected, the shear layer variation causes a variation on the vortex separation of the same wavelength. As Crow (1970) showed, such perturbations of the vortex separation grow exponentially in time, leading to a linking of the vortex pairs and, eventually, to their rapid destruction. However, here the vortices simultaneously diverge which mitigates the growth rate of the instability mechanism. Our ongoing studies will show which of these competing effects will finally determine the vortex decay.

In order to study the effects of the three-dimensionality, we separately performed two 2d simulations which use the shear layer prescribed at

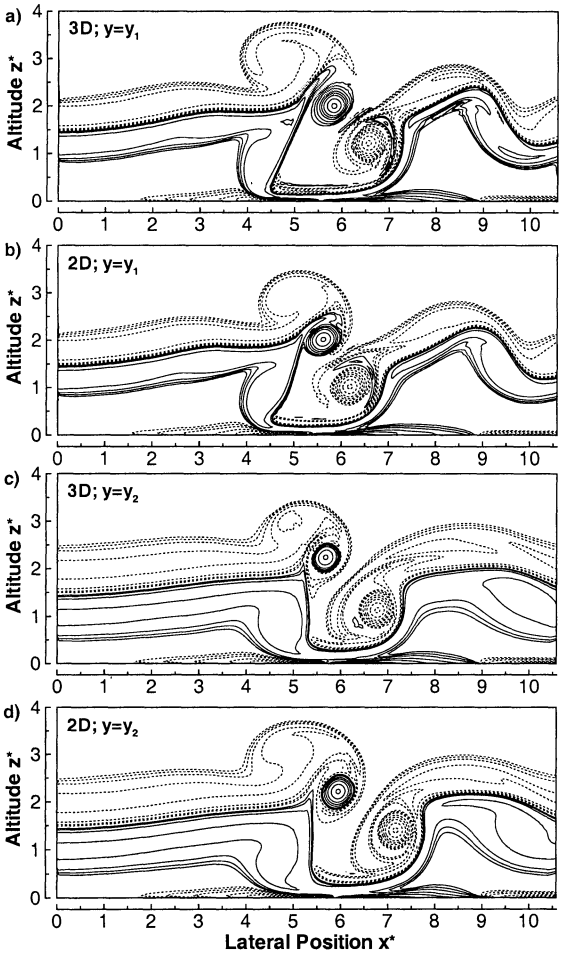

Figure 9: Contour plots of ω_y^* at $t^* = 80.6$ at two axial positions.

$y^* = y_1^*$ and $y^* = y_2^*$ of the 3d case. Figure 9 reveals that differences, as, e.g., the tilting angle of the vortex pair, begin to emerge between 3d and 2d simulations.

CONCLUSIONS

We have conducted two- and three-dimensional simulations in order to investigate phenomena of a counter-rotating vortex pair subjected to various shear layers. We showed that shear layers may cause descending vortices to stall or even to rise. This is initiated by the simultaneous effects of vortex pair tilting and divergence. A tentative explanation of this behaviour is given. In consistence to other works, we find that the vortex whose vorticity is of opposite sign to the shear layer vorticitiy is more likely to rebound. We further showed subtle influence of the shear distribution within the shear layer on the vortex trajectories. With respect to the wake vortex problem, it does not seem feasible in the near future neither to measure nor to forecast the shear distribution accurately enough to reliably predict the vortex trajectories. For the parametrization of shear effects large safety bands for the vortex trajectories will be unavoidable. Spatial shear layer variations, as will always occur in reality, were investigated through a 3d simulation. These cause in an early stage perturbations of the vortex separation which will probably accelerate the vortex decay. Latest results can be found at http://www.pa.op.dlr.de/wirbelschleppe.

REFERENCES

Crow, S. C., 1970, "Stability Theory for a Pair of Trailing Vortices," AIAA-Journal **8**, 2172-2179.

Darracq, D., Moet, H., Corjon, A., 1999 "Effects of Crosswind Shear and Atmospheric Stratification on Aircraft Trailing Vortices," *AIAA 99-0985.*

Dörnbrack, A., Dürbeck, T., 1998, "Turbulent dispersion of aircraft exhausts in regions of breaking gravity waves," *Atmos. Environ.* **32**, 3105–3112.

Greenwood, J. S., Vaughan, J. M., 1988, "Measurements of Aircraft Wake Vortices at Heathrow by Laser Doppler Velocimetry," *Air Traffic Control Quarterly*, **6**(3), 179–203.

Hallock, J. N., Greene, G. C., Burnham D. C., 1998, "Wake vortex research — a retrospective look," *Air Traff. Contr. Q.* **6**, 161–178.

Proctor, F. H., 1996, "Numerical Simulation of Wake Vortices Measured During the Idaho Falls and Memphis Field Programs," *AIAA-96-2496.*

Proctor, F. H., Hinton, D. A., Han, J., Schowalter, D. G., Lin, Y.-L., 1997, "Two Dimensional Wake Vortex Simulations in the Atmosphere: Preliminary Sensitivity Studies," *AIAA-97-0056.*

Robins, R. B., Delisi, D. P., 1990, "Numerical Study of Vertical Shear and Stratification Effects on the Evolution of a Vortex Pair," *AIAA Journal,* **28**,*4, 661–669.*

Schumann, U., Hauf, T., Höller, H., Schmidt, H., Volkert, H., 1987, "A Mesoscale Model for the Simulation of Turbulence, Clouds and Flow over Mountains: Formulation and Validation Examples," Beitr. Phys. Atmosph. **60**, 413–446.